

ANALYSIS OF UPPER EXTREMITY RESPONSE UNDER SIDE AIR BAG LOADING

Stefan M. Duma

Virginia Tech, Impact Biomechanics Laboratory

Brian M. Boggess, Jeff R. Crandall, Shepard R. Hurwitz

University of Virginia, Automobile Safety Laboratory
United States

Kazuhiro Seki, Takashi Aoki

Honda R&D Co., Ltd.

Japan

Paper Number 195

ABSTRACT

Computer simulations, dummy experiments with a new enhanced upper extremity, and small female cadaver experiments were used to analyze the small female upper extremity response under side air bag loading. After establishing the initial position, three tests were performed with the 5th percentile female hybrid III dummy, and six experiments with small female cadaver subjects. A new 5th percentile female enhanced upper extremity was developed for the dummy experiments that included a two-axis wrist load cell in addition to the existing six-axis load cells in both the forearm and humerus. Forearm pronation was also included in the new dummy upper extremity to increase the biofidelity of the interaction with the handgrip. Instrumentation for both the cadaver and dummy tests included accelerometers and magnetohydrodynamic angular rate sensors on the forearm, humerus, upper and lower spine. In order to quantify the applied loads to the cadaver hand and wrist from the handgrip, the handgrip was mounted to the door through a five-axis load cell and instrumented with accelerometers for inertial compensation. All six of the cadaver tests resulted in upper extremity injuries, with comminuted mid-shaft humerus fractures (AIS 3) observed in two tests. Osteochondral fractures of the elbow joint surfaces (AIS 2) were seen in four of the six cadaver tests. Two wrist injuries were observed including a transverse fracture of the distal radius (AIS 2) and an osteochondral fracture of the lunate carpal bone (AIS 2). The results from the six cadaver tests presented in this study were combined with the results from twelve previous cadaver tests. A multivariate logistic regression analysis was performed to investigate the correlation between observed injuries and measured occupant response. Using inertially compensated force measurements from the dummy mid-shaft forearm load cell, the linear combination of elbow axial (FZ) and shear (FX) was significantly ($p = 0.05$) correlated to the observed elbow injuries.

INTRODUCTION

At present, side air bags have been installed in a limited number of cars, and only a few real world crash investigations involving a deployed side air bag have been performed. Langwieder *et al.* (1998) presented one such case in which the vehicle struck a tree close to the right front wheel. Three side air bags were deployed including the right front thorax bag, the right front inflatable tubular structure, and the right rear thorax bag. Although the passenger suffered contusions and sprained his right arm, it was unclear whether the injuries were a result of the deploying door mounted thorax side air bag or the collision itself. Two additional case reports were given by Chidester *et al.* (1998). In the first case, the side air bag was accidentally deployed due to contact with a hockey stick during the act of closing the door. The occupant's upper extremity was bruised, but only as a result of the hockey stick. Little information is given for the second case other than the fact that no injury was recorded. Given the lack of data from currently available case reports, the injury potential from a deploying side air bag must be investigated in the laboratory.

The interaction between a deploying side air bag and the average male upper extremity was evaluated by Kallieris *et al.* (1997), who used the HIII 50th male dummy and five male cadavers. A seat mounted combination head-thorax bag was used with the upper extremity positioned in contact with the seat seam. Only one humerus fracture was observed for the five tests. Thus, it was suggested that there exists a low risk of upper extremity injury during side air bag deployment. It was also noted that the kinematics between the dummy and cadaver were significantly different, highlighting the poor biofidelity of the dummy shoulder joint.

Human volunteer tests were conducted by Igarashi *et al.* (1998) to investigate the interaction between the upper extremity and a deploying side air bag. A combination head-thorax seat mounted bag

was used. While little occupant and air bag inflator data were presented, it was noted that no injuries were recorded. The subjects reported that the impact felt 'like a slight slap.'

A wrist injury was identified in cadaveric tests with side air bags by Jaffredo *et al.* (1998). In this study, the door was equipped with a handgrip. The wrist injury occurred as the side air bag deployed and forced the upper extremity forward, which resulted in the hand becoming entrapped in the handgrip. As the thumb on the cadaver limb was extended, the trapezium carpal bone was fractured. Although no analysis was presented regarding the exact loading of the wrist that induced the injury, this work does present a potential injury mechanism that the handgrip adds to side air bag testing.

A previous study by Duma *et al.* (1998) examined the interaction between the small female dummy upper extremity and small female cadaver upper extremities with a deploying seat-mounted side air bag. In this series of tests, the upper extremity was positioned outboard with the humerus across the seam of the side air bag. The boundary condition on the hand was free as there was no door mounted handgrip. Elbow injuries were the most commonly reported injury. Chondral and osteochondral fractures in the elbow joint were observed for seven of the twelve cadaver tests. Other injuries included a simple fracture of the capitulum and simple fractures on the posterior and right side of ribs 8, 9 and 10. An initial biofidelity analysis showed the dummy as a reasonable predictor of cadaver response as measured by humerus bending moments.

The purpose of this paper is to analyze the upper extremity response under side air bag loading. The results from three dummy and six cadaver tests with a handgrip are presented in this study. Following this, a statistical analysis is presented using these tests combined with the results from nine dummy and twelve previous cadaver tests that used the same side air bags (Duma, 1998).

ANATOMY BACKGROUND

The humerus, radius, and ulna comprise the three long bones of upper extremity and are easily distinguished; however, the anatomy of the elbow is less known. The distal head of the humerus and the proximal ends of the radius and ulna comprise the elbow joint (Figure 1). A much simpler joint than the shoulder joint, the elbow allows flexion of the forearm toward the humerus, extension of the forearm away from the humerus, and one half of the forearm pronation/supination rotations. Closer examination of the elbow joint reveals that flexion/extension is guided by the trochlear notch of

the ulna, which rotates along the trochlea of the humerus. As the forearm reaches full extension, the proximal trochlear notch reaches the joint stop and compresses into the olecranon fossa located on the posterior side of the distal humerus. Of particular importance to the current study is the distal trochlear notch, which is also referred to as the coronoid.

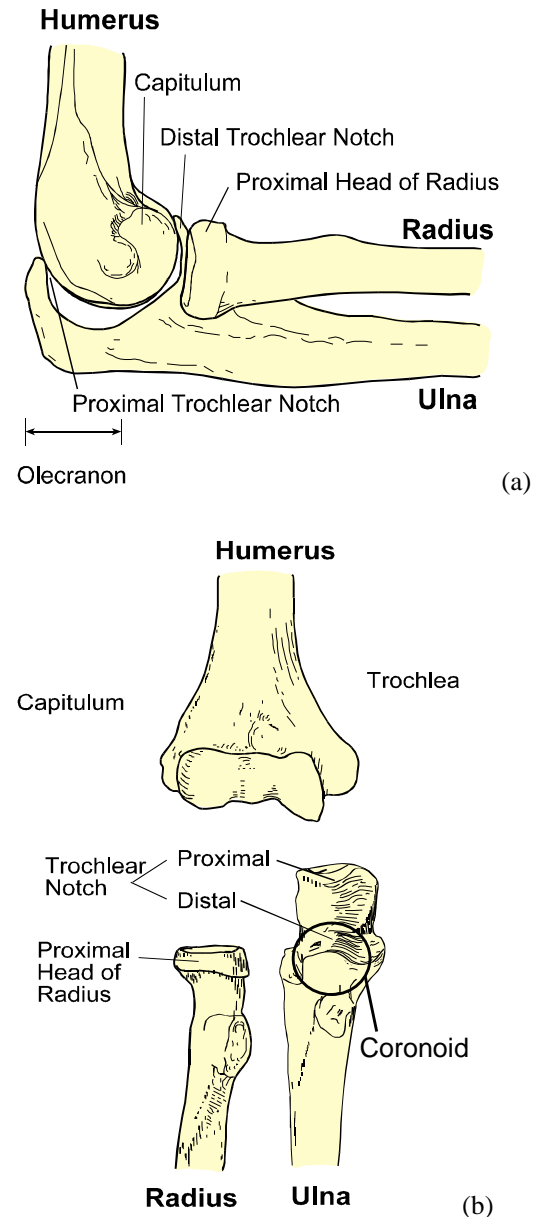


Figure 1. Anatomy of the elbow joint, lateral view (a), anterior view (b).

METHODOLOGY

Side air bag deployments onto dummy and cadaver upper extremities were conducted in a static environment using an actual automobile test buck. The initial occupant position was established from a new multi-body simulation analysis.

Air Bags

Three seat mounted, thoracic side air bags were used that varied only in their level of inflator output. The air bags were prototypes intended for use in a luxury sedan, which contained flexible interior door surfaces with minimal padding. The relative differences in peak pressure and pressure onset rate between the three inflators was measured in a 1 ft³ tank test (Table 1). The inflators utilized hybrid technology, and the bags had two vents on the outboard side.

Table 1. Side air bag inflator characteristics.

Inflator Type	Increase in Peak Pressure Relative to Type A	Increase in Pressure Onset Rate Relative to Type A
A	0%	0%
B	23%	63%
C	54%	160%

Surrogates

Due to their smaller stature, bone structure, and bone mineral loss, women are considered to represent the most vulnerable occupants to out of position air bag loading (Duma, 1999). Therefore, the study presented in this paper investigated the injury potential of side air bags with small female occupants as an estimate of the worst case scenario for drivers or front seat passengers.

For the dummy experiments, the HIII fifth percentile female dummy was used with a new instrumented 5th percentile enhanced upper extremity. The new enhanced upper extremity is a modified version of the Air Bag Interaction Arm that was used in the previous study by Duma *et al.* (1998). Given that the side air bag simulations illustrated the importance of forearm pronation to accurately model the handgrip interaction, the new enhanced upper extremity includes several modifications from the previous version. First, to allow for forearm pronation in the more anatomically accurate location, a single degree of rotation was added proximal to the forearm load cell and a potentiometer was included to record this rotation. This allows rotation along the long axis of the forearm to better simulate the

pronation and supination rotations. A simulation study showed the importance of this included rotation by illustrating that the additional degree of freedom changes the interaction between the hand and the handgrip (Bogges, 2001). Second, the wrist rotations in flexion and extension as well as ulnar and radial deviation were modified to reflect more biofidelic rotational limits and joint stop behavior. Third, two sensors were added to the distal forearm to measure wrist bending moments. The masses of the individual segments were held constant. Finally, a cloth glove was placed on the hand to allow for a similar coefficient of friction between the hand and handgrip compared to that of the cadaver.

The left and right upper extremities of three small female cadavers were tested for a total of six cadaver tests (Table 2). The average weight of 50 kg and stature of 156 mm were nearly identical to the desired weight and stature of the fifth percentile female. Pre-test radiographs of each cadaver were taken and reviewed for possible bone pathology. Any bone anomalies caused the cadaver to be removed from the study. The cadavers were not embalmed and were previously frozen. Post-test radiographs were taken and used in conjunction with a detailed necropsy to identify air bag induced injuries. The cadavers were obtained through the Virginia State Anatomical Board with permission of the family given to conduct biomechanics research. All test procedures were approved by the institutional review board at the University of Virginia.

Table 2. Dummy and cadaver subject anthropometry.

Subject	Sex	Age (years)	Weight (kg)	Stature (mm)
86	Female	69	45.8	1676
90	Female	69	57.0	1447
108	Female	65	46.7	1575
Average		68 ± 2	50 ± 6	1566 ± 115
Dummy	5 th Female	-	48	1525

Instrumentation

The enhanced upper extremity was instrumented with mid-shaft six-axis load cells in the humerus and the forearm. Additional two-axis load cells were located at the distal end of the humerus and forearm. Internally mounted potentiometers measured forearm flexion and forearm pronation. Accelerometers were attached to the forearm and humerus, and magnetohydrodynamic (MHD) angular rate sensors were attached to the spine and humerus to track the upper extremity kinematics (Hall, 1997).

The cadaver instrumentation package was developed to provide comparable response

measurements to those of the Hybrid III. Using specially designed mounts, accelerometer and MHD cubes were attached to the distal radius to measure pronation/supination, proximal ulna to measure elbow flexion/extension, and humerus to measure shoulder rotations. These mounts did not penetrate the cortical bone because a base was created on the bone using a fast curing epoxy, and the mounts were attached to this base using tie-wraps. Using screws that did not intrude into the cortical bone, an accelerometer and MHD cube was attached to the T1 vertebrae to allow for kinematic analysis of the upper extremity relative to the thorax. A strain gage rosette was installed on the mid-shaft humerus that provided for ultimate strain, strain rates, and humerus moments to be calculated. Both dummy and cadaver kinematics were captured with high speed color video (1000 fps).

The handgrip was rigidly attached to the door frame with one contact point via a five-axis load cell. This load cell allowed for the direct observation of contact forces between the occupant's hand and handgrip. Three accelerometers were attached to the handgrip in order to inertially compensate the load for the mass of the handgrip. All load cell and accelerometer data were filtered at CFC 600.

Occupant Positioning

The initial position was determined from side air bag computer simulations in order to maximize the loading of the humerus, elbow, and wrist (Bogges, 2001). A seat mounted thoracic side air bag was approximated by a combination of 5 CVS/ATB ellipsoids. To simulate inflation, the bag originated behind the seat and was forced along a track (slip-joint) by a forcing function that was based on the pressure time-history from preliminary tests and from the observation of a high-speed film of a bag deployment test. The occupant compartment in the CVS/ATB model was constructed with measurements from a drawing of the seat and air bag system supplied by the manufacturer, and from direct measurements of a prototype mid-size vehicle. The seat drawing was used to position the air bag correctly relative to the seat and to size the air bag accurately. The fifth percentile female occupant was used, and the left upper extremity was enhanced to estimate the loads experienced at the centers of the upper arm and forearm segments. These segments were each split into two separate segments connected by locked joints. In addition, segments were added to the wrist and thumb such that the hand could be engaged in the door handgrip, which was also modeled by two ellipsoids.

A parametric study was performed that varied the length, angle, and spacing of the handgrip, as well as the initial position and orientation of the upper extremity. Based on these side air bag simulations and a desire to produce the worst case loading, the door was modified to include a handgrip with a 35° angle and 6 cm space between itself and the door. The simulation results showed extreme sensitivity to the initial hand position and wrist orientation with respect to the handgrip. The selected worst case position for the dummy and cadaver experiments had the occupant positioned slightly outboard with the humerus in contact with the seat back and the forearm on the armrest (Figure 2). The hand was engaged with the handgrip so that the thumb and fingers loosely wrapped around the base of the handgrip.

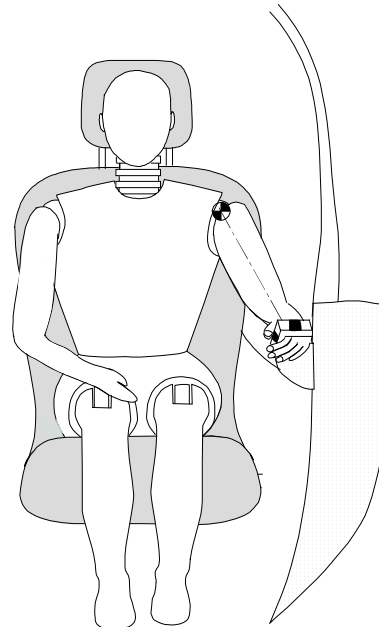


Figure 2. Initial position for the side air bag tests.

The simulation analysis and preliminary dummy tests suggested that a positioning accuracy of ± 3 mm along any axis was the tolerance needed for repeatability. For this reason, a Faro[®] arm (Faro Technologies Inc.) was used for final positioning of the upper extremity in an effort to maintain all measurements within the allowed tolerances. Position landmarks were established on the dummy and cadaver to allow for the same positioning with respect to the air bag for all subjects. A total of three dummy tests were performed, one with each air bag, and six cadaver tests, two with air bag B and four with air bag C.

RESULTS

In both the dummy and cadaver tests, the air bag deployed through the seat seam and drove the humerus and forearm forward, thereby forcing the hand into the handgrip. Although the handgrip interaction for each test was slightly different, the overall upper extremity interaction patterns were similar between the dummy and cadaver tests for each of the different air bags.

Kinematic Data

For the dummy tests, the inertially compensated axial forces at the elbow and wrist were calculated from the forearm load cell, accelerations, and masses (Table 3). The elbow axial force was the summation of the mid-shaft load cell axial force (FZ) and the forearm axial acceleration (AZ) multiplied by 0.74 kg, or the approximate mass of the forearm portion between the elbow and center of the forearm load cell. In the same manner, the elbow shear forces (FX) and (FY) were determined. The wrist resultant force was determined by inertially compensating the

X, Y and Z axis forearm load cell and acceleration recordings for the 0.47 kg portion of the forearm between the load cell and the wrist. Unlike the elbow axial load, all three of the inertially compensated wrist loads were included because the interaction of the wrist with the hand grip included significant off-axis loading. The elbow axial and wrist resultant forces are presented with positive polarities indicating an applied compressive load to the elbow or wrist respectively.

The humerus and elbow loads indicate that the initial punch-out phase of the side air bag deployment resulted in the peak loads for the humerus and elbow which all occurred between 7.0 ms and 13.1 ms after trigger initiation; however, the peak loads in the wrist occurred later in the event as indicated by the timing of the peak wrist and hand grip loads which occurred between 27.1 ms and 32.9 ms (Table 3). This bi-phasic loading was confirmed by analysis of the high speed video which showed the hand sliding up the handgrip between approximately 10 ms and 20 ms. Once the hand contacted the crossbar of the handgrip, appreciable wrist and handgrip loads were observed.

Table 3. Dummy and cadaver loads and observed injuries.

Test	Air Bag	Test Subject	Hand Grip Resultant Force (N)	Time (ms)	Humerus Resultant Moment MX, MY (Nm)	Time (ms)	Elbow Axial Force FZ (N)	Time (ms)	Wrist Resultant Force (N)	Time (ms)
1	A	Dummy	1230	33.0	38	12.2	925	8.2	1019	31.0
2	B	Dummy	1350	27.3	74	11.8	1660	9.8	1021	30.0
3	C	Dummy	2548	27.1	94	8.1	2439	7.0	1415	26.3
Injuries										
4	C	Left 86	1671	19.7	1. Osteochondral fracture of proximal radius head [AIS 2]					
5	C	Left 90	1543	13.7	1. Osteochondral fracture of the medial humerus trochlea [AIS 2] 2. Osteochondral fracture of the coronoid [AIS 2] 3. Osteochondral fracture of the proximal radius head [AIS 2]					
6	C	Left 108	1702	16.5	1. Comminuted mid-shaft humerus fracture [AIS 3] 2. Transverse fracture of the distal radius [AIS 2] 3. Osteochondral fracture of the ulna styloid [AIS 2]					
7	C	Right 86	893	30.2	1. Osteochondral fracture of coronoid [AIS 2] 2. Osteochondral fracture of Lunate carpal bone [AIS 2]					
8	A	Right 90	821	18.5	1. Transverse fracture of the coronoid [AIS 2]					
9	A	Right 108	1293	17.3	1. Comminuted mid-shaft humerus fracture [AIS 3]					

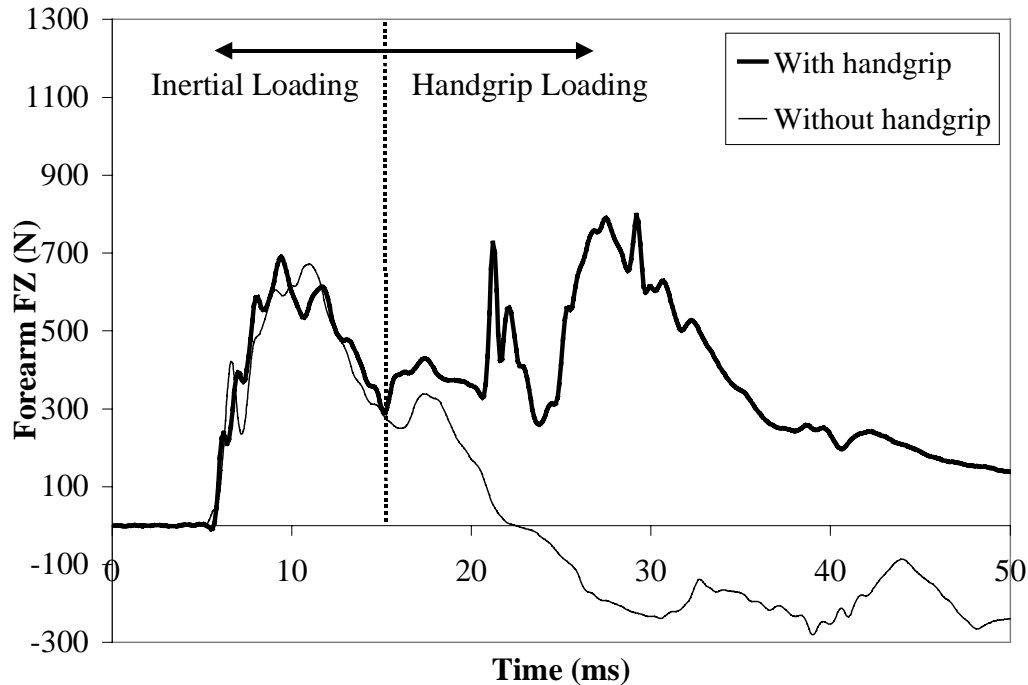


Figure 3. Forearm axial force (FZ) for tests with and without a door mounted handgrip.

When compared to previous experiments without a handgrip, the forearm axial load illustrates the effect of the handgrip on the forearm loading patterns (Figure 3). In both tests with and without a handgrip, the forearm axial load showed an initial peak from 7 ms to 12 ms that was the result of the inertial resistance of the forearm mass as the side air bag deployed forward. In tests without a handgrip, the forearm load then decreased after 12 ms as the forearm translated freely across the body; however, in tests with a handgrip, the forearm is then subjected to a second peak load from 20 ms to 35 ms as the hand became entrapped in the handgrip. The bi-phasic loading of the upper extremity illustrates the primary difference in kinematics between tests with and without a handgrip.

The differences between the inertially compensated wrist loads and the handgrip forces can be attributed to the mass in the hand. For example, test 1 resulted in a wrist load of 1019 N compared to the handgrip load of 1230 N. The increased handgrip load is a result of the hand mass being considered on the handgrip load, but not in the inertial compensation for the wrist loads.

Injury Data

Injuries were observed in all of the six cadaver tests (Table 5). These included comminuted

mid-shaft humerus fractures (AIS 3), elbow joint injuries such as osteochondral fractures of the proximal radius head and coronoid (AIS 2), a distal radius fracture (AIS 2), and chondral fracture of the lunate carpal bone (AIS 1). A discussion of each injury type and corresponding mechanism is presented in the next section.

DISCUSSION

Humerus Fractures - The most severe injuries in this test series were the two AIS 3 mid-shaft humerus fractures from tests 6 and 9. Both tests were performed on subject 108 using the most aggressive air bag C and the least aggressive air bag A. Analysis of post-test radiographs indicated that the two mid-shaft humerus fractures were a result of bending as indicated by the wedge shape fracture patterns (Figure 4). This type of injury was not predicted using the 128 Nm humerus bending criterion when evaluating the dummy humerus moments of 94 Nm and 38 Nm for air bags C and A respectively (Duma, 1999). Moreover, of the six subjects in the previous tests series and the three in this series, subject 108 was the only cadaver out of nine small female cadavers that sustained a humerus fracture from similar side air bag deployments.

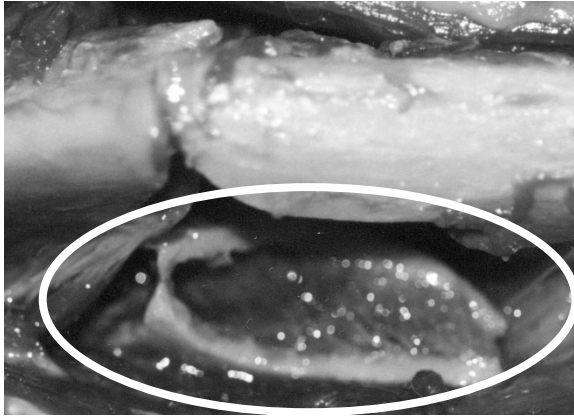


Figure 4. Wedge shape fracture of humerus from test 9.

A closer examination of the subject's bone mineral content explains why subject 108 recorded the mid-shaft humerus fractures. The bone mineral content of each cadaver was determined by using the Osteogram® technique (Osteogram®, San Diego, CA). This procedure uses radiographs of the subject's hand and forearm with a phantom for calibration. The radiograph is then scanned and the bone mineral density is determined and presented as an Osteogram® bone mineral density (BMD) index (Table 4). The BMD index is not the actual bone mineral density, but rather an index number relative to other Osteogram® scans. The more useful output from this technique is the statistically derived bone mineral density T-score and Z-score. The BMD T-score represents the number of standard deviations away from the average the subject's bone mineral content is compared to the average healthy individual between 25 and 50 years. In this application, each subject is compared to healthy females. The positive or negative sign denotes greater or lower bone mineral density respectively. T-scores at -1.0 or greater are considered normal, between -2.5 and -1.0 are considered osteopenia or low bone mineral content, and below -3.0 is considered osteoporotic. The Z-score is the number of standard deviations away from the average bone mineral content of females at the subject's exact age. For example, the bone mineral density of subject 108 was 4.0 standard deviations below the average healthy female between 25 and 50 years. The Z-score indicates that subject 108 was 2.0 standard deviations below the average females of 69 years. In other words, the bone mineral content of subject 108 was lower than 99% of healthy young females, and lower than 95% of 69 year old females.

Table 4. Cadaver bone mineral density.

Subject	Sex	BMD Index	BMD T-score	BMD Z-score
86	Female	74.6	-3.3	-1.0
90	Female	98.3	-1.1	+1.3
108	Female	67.1	-4.0	-2.0
Healthy female between the age of 25 and 50 years		110.0	0.0	

Compared to subjects 86 and 90, the extremely low bone mineral content of subject 108 is the primary reason the two tests with this subject resulted in severe humerus fractures. These two tests with subject 108 suggest that even for the very lowest air bag inflator aggressivity, which resulted in only 38 Nm in the dummy humerus, there exists a small segment of the population that will be vulnerable to humerus fractures from side air bag deployment.

Wrist Injuries - Two of the six tests resulted in wrist injuries with a comminuted fracture of the distal radius and osteochondral fracture of the ulna styloid in test 6 and the other an osteochondral fracture of the lunate bone in the wrist in test 7 (Figure 5). In test 6 the peak handgrip load was 1702 N. Analysis of the high speed video showed the hand engaged in the handgrip directly without appreciable wrist rotation. From the video and the high handgrip load, the injury mechanism for test 6 appears to be axial loading along the distal forearm due to impact with the handgrip. For test 7 the handgrip load was much lower with an 893 N peak. The video showed that the hand interaction with the handgrip was different in test 7 compared to test 6. In test 7 the fingers remained in contact with the handgrip as the wrist was forced into the fully extended position. It is estimated that the injury to the lunate was a combination of axial force and extension bending. There are not enough tests with wrist injuries to date to develop injury risk functions.

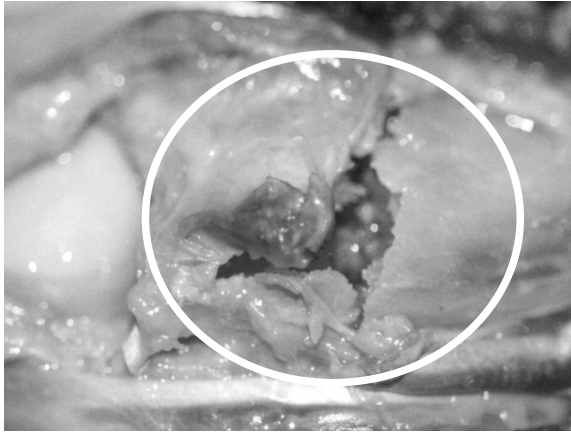


Figure 5. Transverse fracture of the distal radius from test 6.

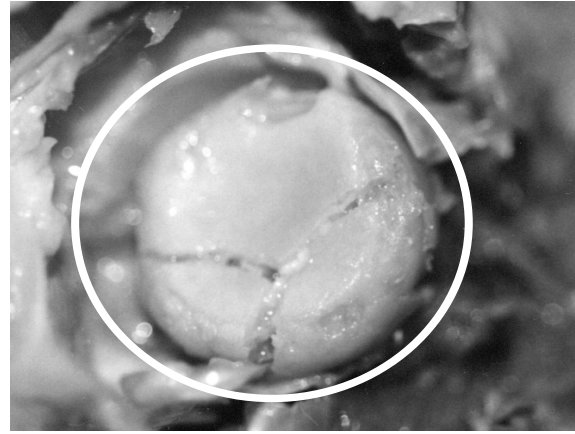


Figure 6. Osteochondral fracture of the radius head from test 5.

Elbow Injuries - Four of the six tests resulted in injuries to the distal side of the elbow joint, or the proximal radius head and coronoid. In previous tests without a handgrip, seven of twelve tests resulted in the same type of injuries to the proximal radius head and coronoid. Although the incidence of distal elbow injuries is similar between tests with and without a handgrip, the elbow injuries in tests with a handgrip were more extensive. In the present study, the elbow injuries included a transverse fracture of the coronoid and osteochondral fractures to the proximal radius head (Figure 6 and 7). These elbow injuries more and deeper fracture lines than the chondral fractures of the coronoid and proximal radius head as observed in similar tests without a handgrip (Duma, 1998). The difference in the fractures is most likely a result of the increased loading as seen in the bi-phasic dummy forearm loads (Figure 3). In other words, there is a double impact in the elbow joint in tests with a handgrip. The first is the initial compression between the distal humerus and the proximal radius head and the ulna coronoid during the punch out phase of the side air bag deployment. In the previous study this impact was labeled as the initial contact injury mechanism (Duma, 1998). The second impact in the bi-phasic loading is also compression of the elbow joint and occurs when the hand becomes entrapped in the handgrip while the air bag is still loading the humerus.

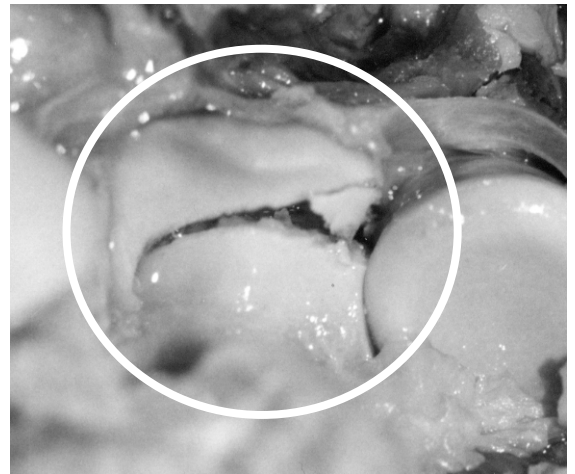


Figure 7. Transverse fracture of the coronoid from test 8.

While the fractures of the mid-shaft humerus and distal radius are obviously serious injuries, the severity of the chondral and osteochondral elbow injuries is not as easily assessed. Chondral fractures involve damage to the cartilage surface of the articulating joint, while osteochondral fractures involve damage to the cartilage and underlying bone. Chondral and osteochondral fractures are difficult to diagnose because they may not appear on a radiograph of the elbow due to the overlapping nature of the trochlea and trochlear notch. Even if detected, they can be very difficult to treat. Due to the low blood supply of cartilage, the prognosis for chondral and osteochondral fractures in the elbow is an arthritic joint that most likely will not heal fully.

It is interesting to note that the two tests that did not result in an elbow injury, tests 6 and 9, were the tests in that resulted in mid-shaft humerus fractures. These humerus fractures may have acted as force limiting structures that failed prior to high or injurious loads being transferred through the elbow joint. The wrist injuries in test 6 could be attributed to a long interaction between the air bag and the forearm after the humerus fractured. In other words, after the humerus fractured in test 6, the elbow load was decreased while the impulse applied from the air bag to the forearm was enough to cause a wrist injury when the hand impacted the handgrip.

STATISTICAL ANALYSIS

Of the eighteen small female cadaver tests with a side air bag, six with a handgrip and twelve without a handgrip, the most common injury location was the distal elbow. Ten of the eighteen tests resulted in injuries on the proximal radius head and coronoid. Due to their prevalence, an analysis of these ten distal elbow joint injuries was performed in order to develop an injury criterion for elbow loading. This grouping is based on the fact that all ten injuries are attributed to compression between the distal humerus and proximal radius head and coronoid as explained in the previous section for bi-phasic loading of the elbow. Moreover, these ten injuries are not attributed to the type of compression loading that may occur from the humerus and forearm reaching the limitation of the elbow joint range of motion.

Logistic regression analysis was used with distal elbow injury and no injury set as the bi-variate response for the eighteen cadaver tests and matched dummy tests. First, a univariate logistic regression analysis was performed. The probability of elbow injury is given by Equation 1 where **a** and **b** are constants and **x** is the occupant anthropometric or response parameter. Cadaver age was a significant contributor to distal elbow joint injuries ($p = 0.003$). Subject mass ($p = 0.84$) and height ($p = 0.73$) were poorly correlated to both injury groups. Of the dummy response parameters, elbow axial force (FZ) yielded the best correlation to distal elbow injury ($p = 0.08$). This risk function is established with values of **a** = -2.83 and **b** = 0.00169 for Equation 1. It predicts a 50% risk of either a proximal radius head or coronoid injury at an elbow axial force of 1680 N. Although not significant at the 95% limit, it does represent a logical risk function for the initial contact injury mechanism.

$$\text{Risk (x)} = \frac{1}{1 + e^{-(a+b \cdot x)}} \quad \text{Equation 1}$$

Next, a multivariate logistic regression analysis was performed on the same eighteen cadaver tests and corresponding dummy tests. For this analysis only two factors were considered for each iterations, but permutations of all combinations were examined. Three constants **c**, **d**, and **e** are needed for the multivariate injury risk function as show in Equation 2. The two occupant anthropometric or response parameters are shown at **x1** and **x2**. A good correlation was found for the combination of cadaver age and dummy elbow axial force (FZ) that has **c** = -18.5, **d** = 0.236, and **e** = 0.00261 ($p=0.002$). A more practical correlation was found with the combination of dummy elbow shear force (FX) and elbow axial force (FZ) that has **c** = -3.14, **d** = 1.079, and **e** = 0.0101 ($p=0.05$). This is a better correlation than was found for elbow axial force alone and suggests that a vertical load component is involved in the production of the elbow injuries.

$$\text{Risk (x)} = \frac{1}{1 + e^{-(c+d \cdot x1 + e \cdot x2)}} \quad \text{Equation 2}$$

CONCLUSIONS

A new computer model was developed to characterize the interaction of an upper extremity under side air bag loading. From the simulations, an enhanced upper extremity was developed with increased biofidelity. In addition, the model was used to develop the worst case loading position for the experimental testing with small female cadavers and the instrumented dummy. All six of the cadaver tests resulted in upper extremity injuries, with comminuted mid-shaft humerus fractures (AIS 3) observed in two tests. Both of the humerus fractures occurred on the same subject. Examination of the subject's anthropometric characteristics revealed that this particular occupant had very low bone mineral content. These two tests with the same subject suggest that even for the lowest air bag inflator aggressivity, which resulted in only 38 Nm resultant bending in the dummy humerus, there exists a very small segment of the population that will be vulnerable to humerus fractures from side air bag deployment.

Two wrist injuries were observed in the present study including a transverse fracture of the

distal radius (AIS 2) and an osteochondral fracture of the lunate carpal bone (AIS 2). While these injuries appear to be the result of axial loading or the combination of axial loading and extension bending, there is no current injury criteria that can be used to interpret this data.

Four of the six tests resulted in osteochondral fractures (AIS 2) to the distal side of the elbow joint, in particular the proximal radius head and the coronoid. Although this incidence is similar to tests without a handgrip, the extent elbow injuries was different in the tests with a handgrip. This was attributed to the bi-phasic loading on the forearm as a result of the initial punch out of the side air bag and the subsequent entrapment of the forearm as the hand interacts with the handgrip.

The test data from the presented series of tests with a handgrip was combined with similar tests with small female cadavers without a handgrip. Of the eighteen small female cadaver tests with a side air bag, six with a handgrip and twelve without a handgrip, the most common injury location was the distal elbow. Ten of the eighteen tests resulted in injuries on the proximal radius head and coronoid. Due to their prevalence, a logistic regression analysis of these ten distal elbow joint injuries was performed. A weak correlation was found between dummy elbow axial force and elbow injury that predicted a 50% risk of injury at 1680 N ($p = 0.08$). A better correlation was found with the linear combination of elbow axial (FZ) and shear (FX) forces. This combination was significantly ($p = 0.05$) correlated to the observed elbow injuries. The inclusion of the elbow shear force (FX) indicates that the elbow injuries are caused not only by an axial force but also by a force that acts vertically relative to the horizontal forearm.

REFERENCES

Bogges, B.M., Sieveka, E.M., Crandall, J.R., Pilkey, W.D., Duma, S.M., Interaction of the Hand and Wrist with a Door Handgrip During Side Air Bag Deployment: Simulation Study Using the CVS/ATB Multi-Body Program, Paper Number 2001-01-0170 SAE Congress and Exposition, Detroit, Michigan, 2001.

Chidester, A.G., Rutland, K.W., Air Bag Crash Investigations, Paper Number 98-S6-O-02, 16th International Technical Conference on the Enhanced Safety of Vehicles, Windsor, Canada, 1998.

Duma, S.M., Crandall, J.R., Hurwitz, S.R., Pilkey, W.D., Small Female Upper Extremity Interaction with a Deploying Side Air Bag, Proceedings of the

42nd Stapp Car Crash Conference, Tempe, Arizona, November, 1998.

Duma, S.M., Schreiber, P.H., McMaster, J.D., Crandall, J.R., Bass, C.R., Pilkey, W.D., Dynamic Injury Tolerance for Long Bones in the Female Upper Extremity, Journal of Anatomy, Vol. 194, Part 3, pp. 463-71, 1999.

Hall, G.W., Crandall, J.R., Klopp, G.S., Klisch, S.M., Pilkey, W.D., Joint Kinematics with Angular Rate Sensors, Journal of Shock and Vibration, Vol. 4, No. 4, 1997.

Igarashi, T., Ehama, M., Sunabashiri, Y., Development of Side Air Bag System For Head & Thorax Protection, Paper Number 98-S8-O-05, 16th International Technical Conference on the Enhanced Safety of Vehicles, Windsor, Canada, 1998.

Jaffredo, A.S., Potier, P., Robin, S., Jean-Yves, L.C., Lassau, J.P., Upper Extremity Interaction with Side Impact Bags, International Research Council on the Biomechanics of Impact, Goteborg, Sweden, 1998.

Kallieris, D., Rizzetti, A., Mattern, R., Jost, S., Priemer, P., Unger, M., Response and Vulnerability of the Upper Arm Through Side Air Bag Deployment, SAE Paper 973323, 41st Stapp International Car Crash Conference, Orlando, Florida, 1997.

Langwieder, K., Hummel, T.A., Anslem, D., The Effect of Airbags on Injuries and Accident Costs, Paper Number 98-S1-W-27, 16th International Technical Conference on the Enhanced Safety of Vehicles, Windsor, Canada, 1998.